Characterizing the Dense Gas in the Eagle and Pelican Pillars

Erin Grand
Marc W. Pound and Lee Mundy
University of Maryland

Introduction

Molecular pillars are formed in HII regions at the boundary between ionized gas and molecular clouds through the effects of photoionization, ablation, and recombination. Pillars like those of the Eagle and Pelican are examples of a phenomenon that is commonly seen wherever molecular clouds are situated near O stars: large "fingers" of dense material that point back at the highly energetic young stars. Proposed formation mechanisms for such pillars generally fall into two broad categories: i) instabilities at the boundary between the cloud and the ionized region which grow with time (e.g. 1,2,3,4) and ii) pre-existing density enhancements (i.e., clumps) which locally retard the ionization front creating cometary shaped protrusions (e.g. 5,6).

We obtained CARMA observations of high density gas in two pillar sources, the Eagle and the Pelican. By studying the underlying mass, density, and velocity distributions in these structures we can uncover evidence for one or both (or neither) of these mechanisms.

Observing with CARMA

Source	Molecule	θ_b (arcsec)	RMS (Jy/beam)	δv (km/s)
Pelican	CS	4.25×3.91	0.18	0.075
Pelican	HCO^+	4.63×4.27	0.15	0.082
Pelican	HCN	4.64×4.28	0.14	0.083
Pelican	N_2H^+	4.42×4.06	0.15	0.079
Eagle	CS	9.01×6.06	0.39	0.075
Eagle	HCO^+	10.02×6.66	0.43	0.082
Eagle	HCN	10.10×6.69	0.42	0.083
Eagle	N_2H^+	9.32×6.34	0.35	0.079

Data Features

We have detailed contour maps for our variety of molecules from which we can derive physical quantities such as mass, density, and velocity distributions within the clouds. (Shown in Figures 1 and 2.)

Given our high resolution, we can see substructure that traces the features in the visible images, so we are confident that we are tracing real structure. There are clear over dense regions in the heads of each of the pillars, as well as in shoulder regions. In all the pillars, we infer that the most dense regions are inside the heads and not right up against the boundary at the head of the pillars with the ionized gas.

The heads of each of the pillars appear to have slightly different shapes among the molecules. For example, the CS map of the Pelican shows a bullet like structure, where as in HCO^+ and HCN the emission is more extended.

Acknowledgments

This work was supported by NIF Concept Development award from DOE/LLNL, #B595751, "Dynamics of the Eagle Nebula" and DOE #DESC0008661, "Scaled Eagle Nebula Experiments on NIF."

CARMA development and operations are supported by the National Science Foundation under a cooperative agreement, and by the CARMA partner universities.

Pelican Nebula

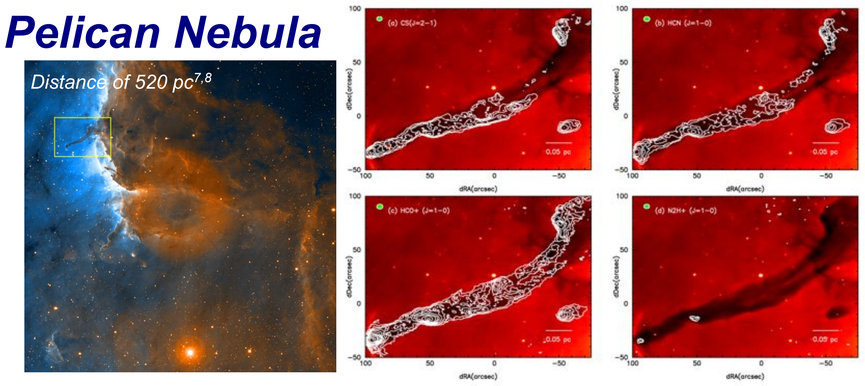

Figure 1: Left: Image of the Pelican nebula with the area mapped indicated by the box. Right: Integrated emission over all velocities for CS, HCN and HCO^+ and N_2H^+. The white contours start at 0.06 Jy/beam km/s and go up to 0.9 Jy/beam km/s.

Eagle Nebula

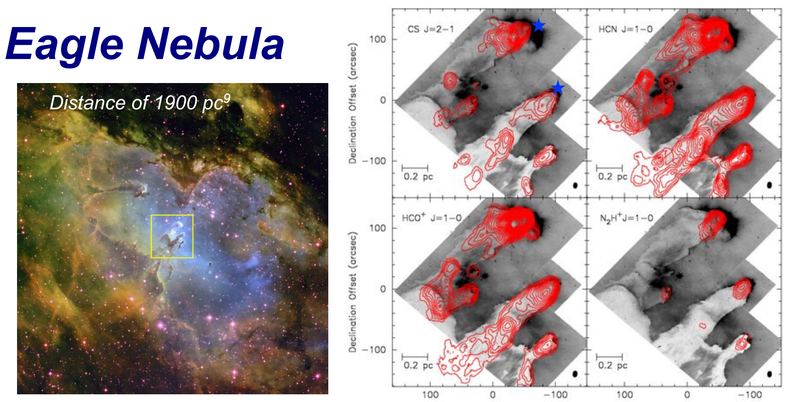

Figure 2: Left: Image of the Eagle nebula with the area mapped indicated by the box. Right: Integrated emission over all velocities maps for CS , HCN, HCO^+ and N2H+. The blue stars represent the locations of small protostars in the heads of the pillars. The red contours start at 0.8 Jy/beam km/s and go up to 20 Jy/beam km/s.

Density

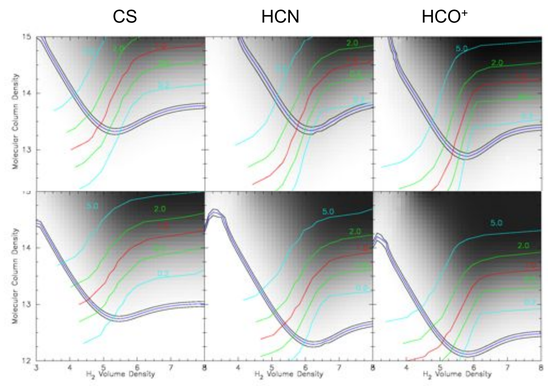

Figure 3: We use LVG to calculate molecular column density and H_2 volume density as a function of temperature (greyscale) and opacity (colored contours). The dark blue temperature lines represent the observed intensity at the head of the second pillar of the Eagle (top row) and the head of the Pelican (bottom row). The black lines are +/- 10% of the blue. We measure a kinetic temperature T_K = 57K for the Eagle and T_K = 27K for the Pelican from ^{12}CO spectra.

We find that the HCN satellite line ratios are consistent with HCN being optically thin. This constrains the molecular column density and provides a lower limit for the H_2 volume density. Using the lower limit of the volume density, and assuming the depth of the pillars is comparable to their width, we can calculate a H_2 column density and take the ratio to the molecular column density to get a fractional abundance. The derived values are given in the table below.

Source	Molecule	Molecular Column Density cm^{-2}	H_2 Volume Density cm^{-3}	Size pc	H_2 Column Density cm^{-2}	Average Fractional Abundance
Eagle	CS	$10^{13.3-13.8}$	$> 10^5$	0.12	1×10^{22}	5×10^{-10}
Eagle	HCN	$10^{13.3-13.8}$	$> 10^6$	0.12	6×10^{22}	4×10^{-11}
Eagle	HCO^+	$10^{12.8-13.5}$	$> 10^{5.5}$	0.12	4×10^{22}	3×10^{-11}
Pelican	CS	$10^{12.7-13.0}$	$> 10^{4.8}$	0.06	4×10^{22}	2×10^{-10}
Pelican	HCN	$10^{12.3-12.5}$	$> 10^{5.5}$	0.06	4×10^{23}	7×10^{-12}
Pelican	HCO^+	$10^{12.0-12.2}$	$> 10^{5.3}$	0.06	1×10^{23}	1×10^{-11}

Dynamics of the Pillars

From position-velocity diagrams we can derive the magnitude and direction of the velocity gradients in the pillars. The Pelican has a velocity gradient of -1.9 km/s/pc, and the Eagle pillars have gradients of -10.43, +16.7, +2.1 and -1.8 km/s/pc for the upper first pillar, lower first pillar, second pillar and, third pillar respectively. Figures 4 and 5 show that the velocity-position cuts appear similar among the different molecules.

The position-velocity information (Figure 4) shows three parts to the Pelican pillar. The head, a second dense feature, and a third less dense tail component. The head (left-most dense feature) and first tail seem to have a slightly positive gradient, where as the other two structures have negative velocity gradients.

The velocity structure along the first pillar of the Eagle (Figure 5) implies that the top part of the pillar is a separate structure from the lower part, rather than being one continuous pillar as would appear in the Hubble image.

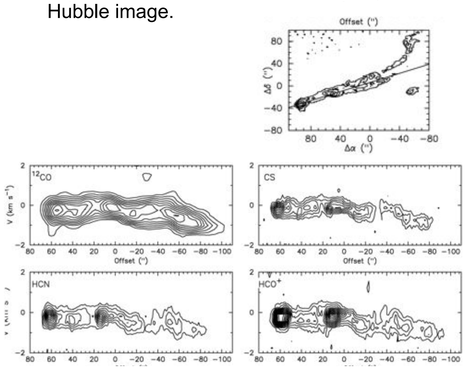

Figure 4: Position-velocity diagram for the Pelican shown ^{12}CO, CS, HCN, and HCO+. The cut is displayed in the top right corner.

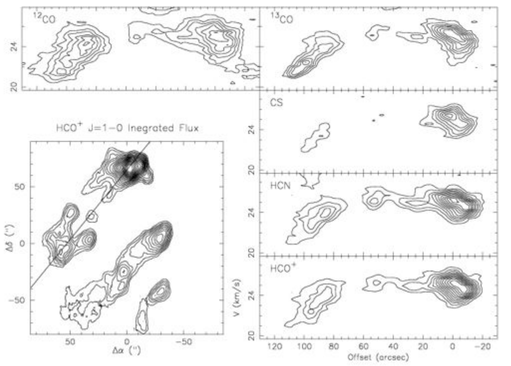

Figure 5: Position-velocity diagram for a cut through the first pillar of the Eagle shown for ^{12}CO, ^{13}CO, CS, HCN, and HCO+. The cut is displayed in the lower left corner.

Comparison to "Cometary" Model

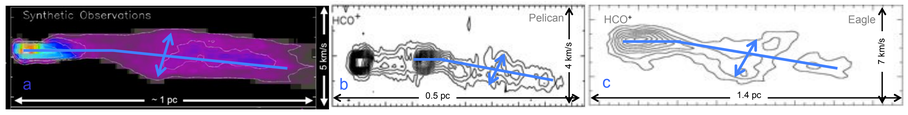

Figure 6a: Position-velocity cut through a synthetic pillar observation showing a velocity change and increase in width in the tail.[10]
Figure 6b: Position-velocity cut through the Pelican pillar in HCO+ for comparison.
Figure 6c: Position-velocity cut through the second pillar in the Eagle in HCO+ for comparison.

In both the Eagle and the Pelican pillars, the velocity stays mostly constant through the head and then changes in the tail. This is a feature reminiscent of synthetic observations of pillars formed in "cometary" model simulations. The effect is demonstrated by the blue lines. The velocity is flat through the head, then drops in the tail. The line widths broaden in the tail by 3 km/s in the model, 1 km/s in the Pelican and 3 km/s in the Eagle.

Conclusions

The pillars are coherent gas structures, with over dense heads, less dense tails and complex substructure. The heads of the pillars have volume densities n(H2) > 10^5 cm-3 and column densities $N(H_2) >\sim 10^{22}$ cm^{-2}.

The structure and kinematics of the pillars are consistent with the "cometary" scenario for their creation. In that scenario, the head is dense; the material directly behind the head has lower relative velocity than that in the tail since it is protected from the ionization front. Gas in the tail is more turbulent as the front wraps around an impacts the gas from the sides.

The velocity patterns in the data match these expectations, with a gradient running from head to tail and a broadening of the velocity width in the tail. In fact, previous synthetic observations of radiative hydrodynamic models of the "cometary" scenario fit our data surprisingly well. While our observations lends support for this particular model, we cannot yet rule out competing radiative instability models for pillars due to a lack of detailed model velocity fields.

1. Spitzer 1954, ApJ, 120, 1 • 2. Frieman 1954, ApJ, 120, 18 • 3. R.J.R. Williams et al. 2001, MNRAS, 327, 788-798 • 4. Mizuta et al. 2005, ApJ, 647, 1151 • 5. Reipurth 1983, A&A, 117, 183 • 6. Bertoldi & McKee 1990, ApJ, 354, 529 • 7. Laugalys et al, 2006a, Baltic Astron, 15, 483 • 8. Straizys et al 1989, Baltic Astron, 8, 335 • 9. L.A. Hillenbrand et al, 1995, AJ 106, 1906 • 10. Pound, et al, 2007, A&SS 307, 187